VANADIUM AND TITANIUM OXIDES PREPARED BY HYDROLYSIS OF ALKOXIDES AS INSERTION ELECTRODES IN LITHIUM CELLS WITH POLYMERIC ELECTROLYTES

M. G. MINETT and J. R. OWEN

Department of Chemistry, University of Salford, Salford M5 4WT (U.K.)

(Received September 4, 1989; in revised form January 31, 1990)

Summary

Single and mixed oxides of titanium and vanadium, prepared by hydrolysis of alkoxides using a sol–gel technique, have been evaluated as positive electrodes in all-solid-state lithium cells. These oxides were shown to have similar gravimetric capacities to, but higher rate capabilities than, the established lithium insertion electrode phase V_6O_{13}.

1. Introduction

Insertion electrode compounds constitute the most attractive positive electrode materials to be coupled with lithium in non-aqueous, high energy, secondary cells [1, 2]. The proposal by Armand *et al.* [3] that a lithium-ion conducting polymer, such as poly(ethylene oxide) (PEO) complexed with a lithium salt, could be employed as a solid electrolyte in lithium cells coupled with insertion compounds, has led to an intense research effort directed towards the production of an all-solid-state lithium cell [4 - 9]. The attractive features of such a cell include ease of fabrication, excellent packaging efficiency and long shelf and cycle life. The most widely studied insertion compounds in cells of this type are crystalline transition metal chalcogenides, for example V_6O_{13}, TiS_2 and $Li_{1+x}V_3O_8$. Due to their low electronic and ionic conductivities, these electrode materials are often mixed with ionic conductors (for example PEO) and electronic conductors (for example acetylene black) to form a composite electrode structure. However, structural and morphological changes occur in this composite on cell cycling due to expansion and contraction of the insertion electrode material on lithium insertion and extraction. This results in a capacity loss of the cell during cycling which is believed to arise as a result of the disruption of the electronic and ionic conducting pathways [10].

Insertion electrode compounds with amorphous structures, for example MoS_3 [11], and Cr_3O_8 [12], have recently been attracting more attention in lithium–organic-electrolyte cells, since in certain cases they have been found to outperform their crystalline counterparts. One of the most widely studied

0378-7753/90/$3.50

systems of this type is V_2O_5 glasses prepared by using network formers, for example P_2O_5 [13], B_2O_3 [14] and TeO_2 [15]. V_2O_5–P_2O_5 glasses of this type show superior rechargeability and cycleability when compared to crystalline V_2O_5; this superior performance is believed to be a consequence of a variation in bond lengths which results in a structure which is more flexible to the insertion and extraction of lithium [16].

A more recent example of an amorphous insertion electrode material is a V_2O_5 xerogel prepared via the sol–gel process [9]. The xerogel was cycled in a lithium–polymeric electrolyte cell 46 times with only minor capacity losses. The sol–gel method of preparing materials has emerged as a powerful technique in recent years. Sol–gel processes have been exploited in making a wide range of materials, especially glasses, glass ceramics, and oxides of practical importance [17]. A common technique utilised for preparing metal oxide gels is the hydrolysis of metal alkoxides. The use of mixed alkoxide solutions makes possible the synthesis of novel structures which cannot be produced by more conventional preparative routes. An example of this type of mechanism has been used by Boilot *et al.* [18] in the preparation of superionic conductors from mixtures of silicon alkoxides with lithium and transition metal alkoxides.

The sol–gel technique can be seen to offer many potential advantages in the production of insertion electrode materials. These may be summarised as follows:

(i) Precipitation of oxides in this manner can give small (submicron) particle size with consequently high surface area.

(ii) Low processing temperatures are possible in comparison to previously reported techniques for the preparation of insertion electrode materials.

(iii) Materials can be formed in thin film configuration suitable for direct use in all-solid-state polymeric electrolyte cells.

(iv) It is possible to freeze polymeric species into the oxide matrix, thus producing microcomposite materials with unique properties, for example concurrent electronic and ionic conductivity [19].

In this paper we have investigated the possibility of preparing multicomponent oxide systems using transition metal alkoxides as the precursor materials. Vanadium and titanium alkoxides were chosen as the precursor materials. Vanadium was chosen since its oxide has already been demonstrated to exhibit high capacity. Titanium was chosen as a structure breaker as its precursor alkoxide was readily available and it is of a similar ionic size to vanadium. Titanium oxide also has the advantage over inert network formers such as B_2O_3 of having a demonstrated reversible capacity, as in lithium/TiO_2 (anatase) cells. Mixed oxide systems of this type have been investigated previously by Hirashima *et al.* [20] but no electrochemical characterisation of the mixed oxides produced was attempted.

It should also be noted here that vanadium–titanium mixed oxide systems have been investigated previously as catalysts for a number of oxidation reactions [21]. These mixed oxides are generally prepared by high tem-

perature annealing of mixtures of the single oxides. Preparation of a mixed oxide of this type by a sol–gel route may also prove interesting for catalytic applications.

2. Experimental

2.1. Materials preparation

The technique used for the preparation of the alkoxides was adapted from the method reported by Boilot *et al.* [18]. The alkoxide precursor compounds used were titanium tetraisopropoxide, $Ti(OC_3H_7)_4$ and vanadyl triisopropoxide, $VO(OC_3H_7)_3$, ex Alpha Ventron chemicals.

The alkoxide precursor (5 cm^3 of single or mixed alkoxide, used as supplied) was diluted to 10 cm^3 with solvent (ethanol AR grade ex BDH, used as supplied) inside an argon-filled glove box ($H_2O < 5$ ppm). The mixtures were allowed to stand for approximately 1 h, removed from the dry box and poured into a small Petri dish (diameter 50 mm) which was covered with a sheet of filter paper. The mixtures were allowed to stand for 16 h and dried at 120 °C under vacuum (<1 Torr) for 1 h. The resulting powders were annealed at 120 - 600 °C inside a furnace (in air) for 8 h. The effects of the annealing temperature and the ratio of vanadium:titanium alkoxides on the properties of the powders formed were investigated.

2.2. Materials characterisation

X-ray diffractograms of the oxides were taken using a Philips PW 1840 X-ray diffractometer (Cu Kα radiation). The oxidation state of vanadium in the oxide materials was determined by redox titration [22]. Differential thermal analysis (DTA) (using a DuPont 900 thermal analyser, 25 - 600 °C, 10 °C min^{-1}) and thermogravimetric analysis (TG) (using a Stanton-Redcroft TG-750, 25 - 600 °C, 10 °C min^{-1}) were performed on selected oxide samples in both flowing nitrogen and air. The surface areas of the oxide powders were measured by the BET method using a Micromeritics analyser, model 2205. Electron micrographs of the oxide powders were taken on a JEOL JSM-35 electron microscope. EDAX measurements were taken using a Philips 505 scanning electron microscope with a Philips 9100 EDAX attachment. Elemental distribution maps were made by comparison of the titanium Kα and vanadium Kβ X-ray lines (the stronger vanadium Kα line was not monitored since it overlapped with the titanium Kβ line). Electronic conductivities of the oxides were measured on pressed discs (0.2 g of oxide powder pressed at 10 tonnes for 60 s to produce 1 cm^2 discs) by the method of Van der Pauw [23] using a Jandel commercial 4-point probe.

2.3. Constant current cell cycling

A series of small scale, sandwich-type cells of area 1.5 cm^2 was constructed. The cells consisted of: lithium foil (100 μm film ex Lithco — a large excess of lithium was used so that the capacity of the cells would be

limited by the positive electrode); polymer electrolyte (2×50 μm thick discs, prepared by casting a 2% solution of PEO–$LiCF_3SO_3$ ([EO units]:Li = 8:1) in acetonitrile and drying under vacuum (<1 Torr) to form free-standing films); positive electrodes were prepared by ball-milling the insertion oxide powders (0.684 g) together with Shawinagan acetylene black (0.05 g) in 10 cm^3 of a 2% solution of PEO–$LiCF_3SO_3$; the resulting dispersions were cast onto a poly(ethylene) substrate and dried to form a free-standing film of approximately 60 μm thickness. The positive electrode and the polymer electrolyte films were cut into discs and dried under vacuum (<1 Torr) in a Buchi furnace at 120 °C for 24 h. The discs were transferred to an argon-filled glove box (<5 ppm H_2O) (NB, cell assembly was performed in a different drybox to that used for oxide preparation in order to avoid solvent contamination of the lithium). Sandwich-type cells were assembled in a specially designed, air- and water-tight, cell holder and squeezed together under spring pressure (0.20 - 0.25 kg cm^{-2}). The cells were enclosed in glass sleeves and placed into a thermostatically controlled heater (located inside the dry box) where they were heated to 120 ± 2 °C. Constant current cell cycling experiments were made using an in-house built 8-channel constant current supply controlled by an IBM personal computer. For comparative purposes V_6O_{13} was also tested in the same manner as outlined above: the V_6O_{13} sample (supplied by Chloride Advanced Research [22]) was prepared by thermal decomposition of ammonium metavanadate; subsequent analysis showed a stoichiometry of $VO_{2.19}$ and a surface area of the oxide of 7 m^2 g^{-1}.

3. Results and discussion

3.1. Titanium oxides

Figure 1 shows the changes in crystal structure of titanium oxides with annealing temperature. After annealing at 400 °C, titanium oxide crystallised in the anatase form [24]; annealing at 600 °C resulted in a partial transformation of anatase to rutile [25]. Figure 2 shows that a high capacity for the sample annealed at 400 °C was obtained in comparison to the samples annealed at 120 and 600 °C. Similar capacity trends were also noted during cell cycling (Table 1) with the samples annealed at 120 and 600 °C showing poor reversibility. The results for the crystalline titanium oxides show the same trends as those reported by other workers [26 - 29] and have been explained by a low diffusion coefficient for lithium in the rutile structure. Increased crystallinity in anatase TiO_2 has been shown to retard lithium diffusion [29]; the poor performance of the sample annealed at 120 °C was therefore very disappointing. A suggested explanation for this result may have been an extremely low electronic conductivity due to incomplete calcination of the oxide (poorly formed oxides may contain end groups such as Ti–OH or Ti–OR which would block the normal conductivity route via Ti–O–Ti bridges).

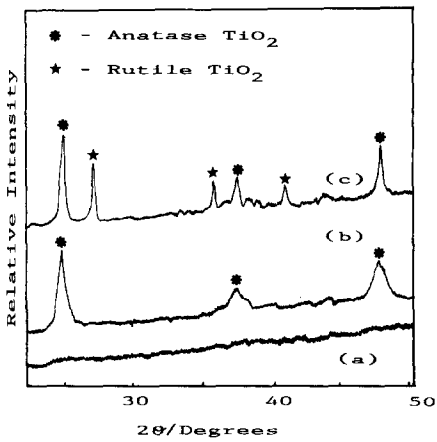

Fig. 1. Change of X-ray diffraction pattern with annealing temperature for titanium oxides annealed at (a) 120, (b) 400, (c) 600 °C.

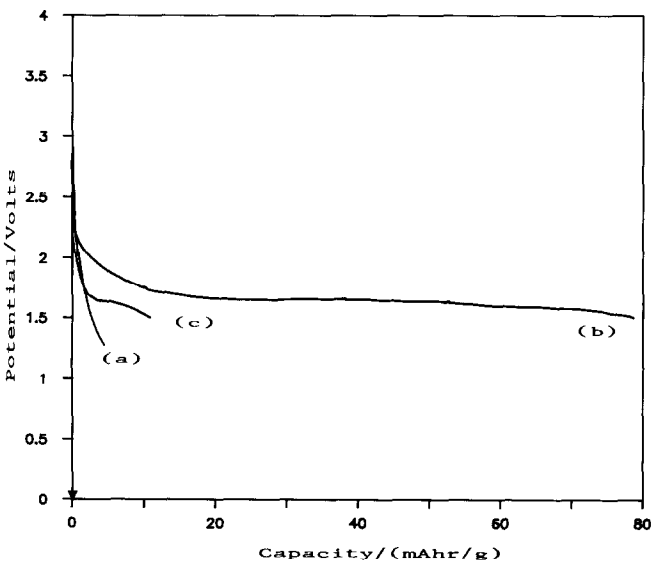

Fig. 2. Variation of cell capacity with annealing temperature for titanium oxide cells discharged at 0.033 mA cm^{-2}; annealed at (a) 120, (b) 400, (c) 600 °C.

3.2. *Vanadium oxides*

The effect of air annealing on the crystallinity of the vanadium oxide samples is shown in Fig. 3. The degree of crystallinity increased gradually with temperature from 120 to 600 °C, when the sample was mainly orthorhombic V_2O_5 [30]. Incomplete calcination of samples annealed below 250 °C was demonstrated in the TG analyses (Fig. 4) by mass loss above that temperature, and chemical analysis (Table 2) indicated a lower

TABLE 1

Summary of cycling data for titanium oxides (0.333 mA cm^{-2} discharge, 0.083 mA cm^{-2} charge, 3.0 - 1.7 V)

Annealing temperature (°C)	*OCV* (initial) (V)	Capacity (mA h g^{-1})	
		Cycle 1	Cycle 25
120	2.940	2(0.01)[a]	
400	2.855	60(0.18)	90(0.27)
600	2.754	30(0.09)	

[a]Results in brackets denote the number of inserted lithium ions per TiO_2 molecule.

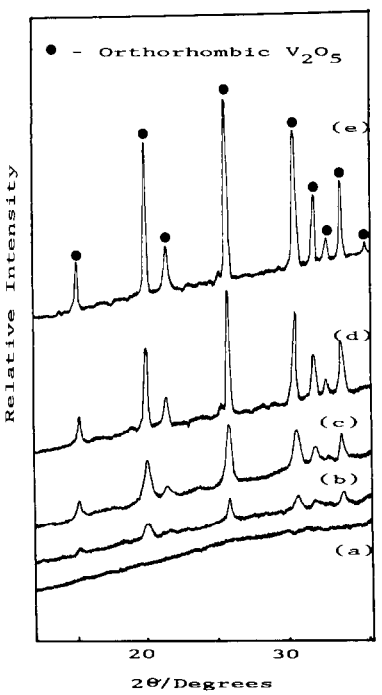

Fig. 3. Change of X-ray diffraction pattern with annealing temperature for vanadium oxides annealed at (a) 120, (b) 180, (c) 250, (d) 400, (e) 600 °C.

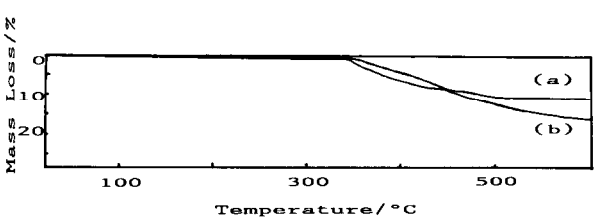

Fig. 4. TG curves of vanadium oxide in (a) air and (b) nitrogen.

TABLE 2

Variation of vanadium oxidation state with temperature of annealing in air[a]

Temperature (°C)	120	180	250	400	600
Vanadium oxidation number	—	3.9	4.2	4.95	4.95
X-ray diffraction pattern	A	A	A/C	C	C
Colour	black	black	orange	yellow	yellow

[a]A = amorphous, C = crystalline.

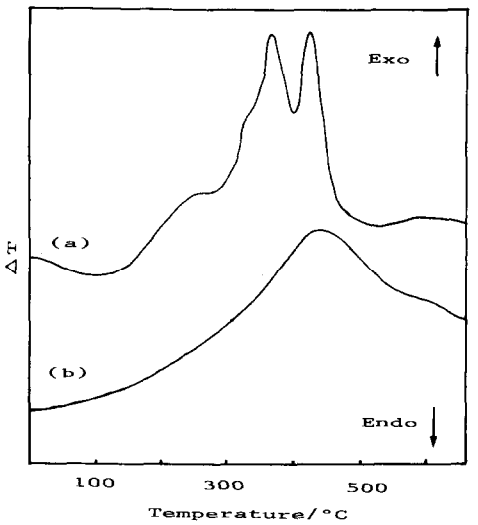

Fig. 5. DTA curves of vanadium oxide in (a) air and (b) nitrogen.

oxidation state of vanadium in these cases. Also, DTA traces (Fig. 5) in the presence of oxygen showed exotherms suspected to be due to the burning of residual organics as well as heat of crystallisation. Given the possibility of oxidation of these organics during the redox titration, the calculation of the vanadium oxidation state in the samples annealed at 180 and 250 °C should be viewed with caution, although the colour of the samples implied significant reduction below V^{5+}. A comparison of identical samples annealed in air at 120 °C, analysed by TG in air and nitrogen, respectively, showed a final mass for the nitrogen-treated sample of 93.3% compared with that analysed in air. Taking the molar mass ratio V_2O_4/V_2O_5 as 0.912 the vanadium oxidation state may be calculated to be 4.2. However, the broad exotherm in the DTA trace in nitrogen implied an internal redox process between V^{5+} and the organic material, so that the calculated stoichiometry of $VO_{2.1}$ represents the maximum degree of reduction of vanadium in the samples used in capacity measurements. Electronic conductivities of the vanadium oxide samples are shown in Table 3. The conductivity values were in the range of those reported by other workers [31].

TABLE 3

Conductivities (measured on 4-point probe) of mixed oxide samples (10^{-2} S m^{-1})

Annealing temperature (°C)	Titanium content (mol%)				
	0	11	27	53	100
120	0.20			$<10^{-2}$	$<10^{-2}$
250	6.92			0.67	$<10^{-2}$
400	13.59	14.70	4.97	1.10	$<10^{-2}$
600	8.01			4.29	$<10^{-2}$

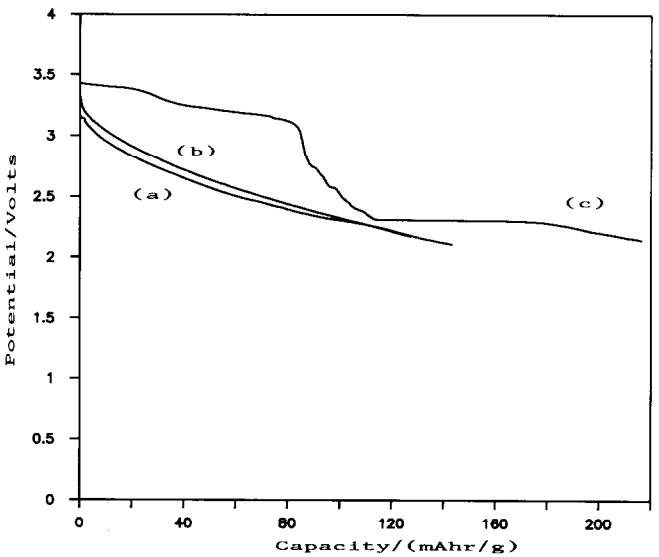

Fig. 6. Variation of cell capacities with annealing temperature (a) 120, (b) 250, (c) 600 °C for vanadium oxide cells discharged at 0.033 mA cm^{-2}.

Examples of slow (0.033 mA cm^{-2}) discharge curves for vanadium oxides are shown in Fig. 6. Predominantly crystalline V_2O_5 samples (annealed above 400 °C) gave a stepped discharge curve characteristic of phase changes as reported by other workers [32, 33]. Amorphous and partially crystallised samples gave smooth, gradually declining discharge curves typical of one-phase behaviour as commonly reported for other amorphous insertion electrode materials [11, 12]. Table 4 summarises cycling data for vanadium oxide cells. On cycling between 3.2 and 2.2 V, a general trend of increasing capacity with annealing temperature could be seen with no apparent degradation of capacity with cycle number. In fact, small increases in capacity were noted over the first three cycles. This effect was thought to be associated with an improving interfacial contact with time

TABLE 4

Summary of cycling data for vanadium oxides (0.333 mA cm^{-2} discharge, 0.083 mA cm^{-2} charge)

Annealing temperature (°C)	*OCV* (initial) (V)	Capacity (mA h g^{-1})			
		3.2 - 2.2 V		3.2 - 1.7 V	
		Cycle 1	Cycle 10	Cycle 1	Cycle 10
120	3.577	30(0.20)[a]	44(0.30)	196(1.33)	110(0.75)
250	3.467	23(0.16)	48(0.33)	195(1.32)	116(0.79)
400	3.494			495(3.23)	232(1.58)
600	3.481	97(0.66)	111(0.75)	525(3.56)	235(1.60)

[a]Results in brackets denote the number of inserted lithium ions per vanadium oxide formula unit (assumed to be V_2O_5).

and was seen in all cell tests reported in this paper. Extending the discharge voltage limit down to 1.7 V resulted in an approximately 4 times increase in capacity for all cells; however, this rapidly declined in 1 - 2 cycles, after which a steady cycling capacity, approximately double that achieved for discharge to 2.2 V, was maintained. This effect has been widely reported as occurring in crystalline V_2O_5 [32, 33] and is due to a structural reorganisation. It is interesting to note that the capacity degradation in the amorphous samples followed a similar pattern, suggesting a similar mechanism for capacity loss, despite the fact that the shape of the discharge curve (Fig. 6) suggests a disordered phase was present throughout the composition range studied.

3.3. Mixed vanadium/titanium oxides

3.3.1. Effect of annealing temperature

X-ray diffractograms (Fig. 7) show that mixed vanadium/titanium oxide systems (containing 53 mol% titanium) remained largely amorphous until annealed at temperatures in excess of 400 °C, when crystallisation to orthorhombic V_2O_5 and rutile TiO_2 occurred. Crystallisation was therefore hindered in the mixed oxide system. This is a known phenomenon caused by an increased requirement for diffusion for the crystallisation processes to occur in the mixed system. Scanning electron micrographs of the oxides corresponding to the X-ray diffraction patterns in Fig. 7 are shown in Fig. 8 with their corresponding surface areas shown in Table 5. At 120 °C, the oxide powder consisted of particle sizes of the order of 1 μm and below, with some larger agglomerates. When the temperature was increased to 400 °C, the proportion of particles of the finer particle sizes increased and evidence of some crystallisation could be observed; this corresponded to an increase in surface area. When the annealing temperature was increased to 600 °C the particles crystallised further, resulting in reduced surface area. EDAX analysis showed an even concentration of vanadium and titanium

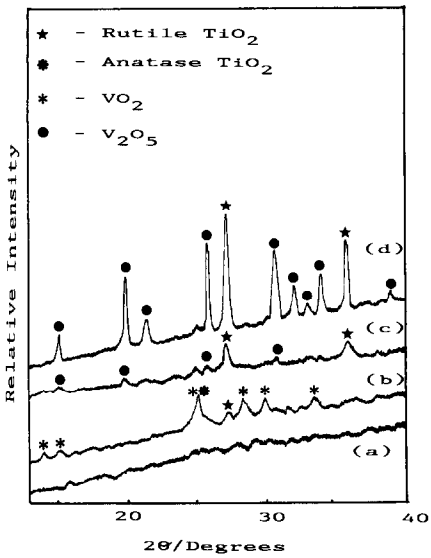

Fig. 7. Change of X-ray diffraction pattern with annealing temperature for mixed vanadium/titanium oxide (53 mol% Ti) annealed at (a) 120, (b) 250, (c) 400, (d) 600 °C.

across the amorphous samples indicating a homogeneous dispersion on a scale lower than the resolution of the instrument (1 μm). Electronic conductivities were slightly lower than those of vanadium oxide but increased with annealing temperature.

Results for a slow (0.033 mA cm^{-2}) discharge are shown in Fig. 9. The crystalline material, annealed at 600 °C, exhibited a sharp step in the discharge curve similar to that found in crystalline V_2O_5. This step occurred at approximately half the capacity of that in crystalline V_2O_5; since the mixed oxide was composed of approximately 50% vanadium oxide, this suggests that lithium was inserted preferentially into V_2O_5 during initial discharge. The non-crystalline samples, annealed at lower temperatures, gave smooth discharge curves typical of those found in amorphous compounds. Constant current cycling experiments (Table 6) show that the highest capacity was achieved in the sample annealed at 400 °C. The differences in results may have been due to changes in the crystallinity of the samples. However, other factors such as differences in surface area cannot be ignored, since the highest capacity was achieved from the sample with the highest surface area.

3.3.3. Effect of titanium: vanadium ratio

The X-ray diffractograms in Fig. 10 show that the mixed oxide system remained poorly crystalline (on annealing at 400 °C) on addition of as little as 11 mol% vanadium. The DTA curves (Fig. 11) further illustrate the effect of titanium content on the suppression of the crystallisation processes in vanadium oxide. From slow (0.033 mA cm^{-2}) discharge curves (Fig. 12), it can be seen that, as the percentage of titanium in the mixed oxide was

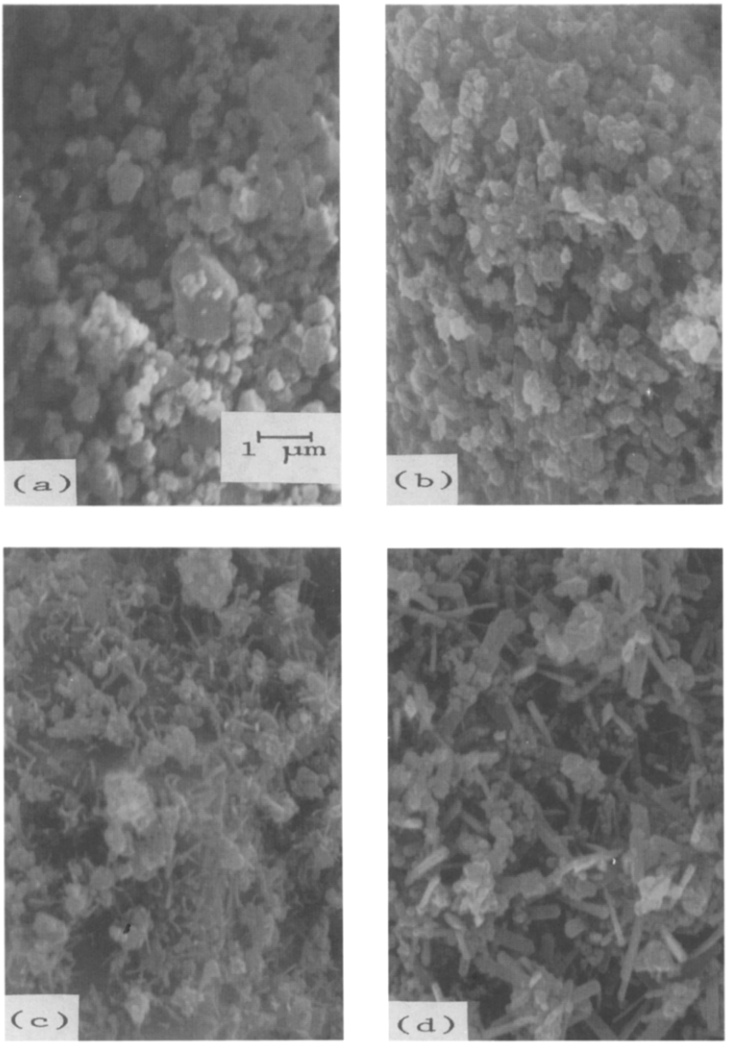

Fig. 8. Scanning electron micrographs of mixed vanadium/titanium oxides (53 mol% Ti) at (a) 120, (b) 250, (c) 400, (d) 600 °C.

TABLE 5

Variation of surface areas of mixed vanadium/titanium oxides (53 mol% Ti) with annealing temperature

Temperature (°C)	120	250	400	600
Surface area ($m^2 g^{-1}$)	9	18	26	5

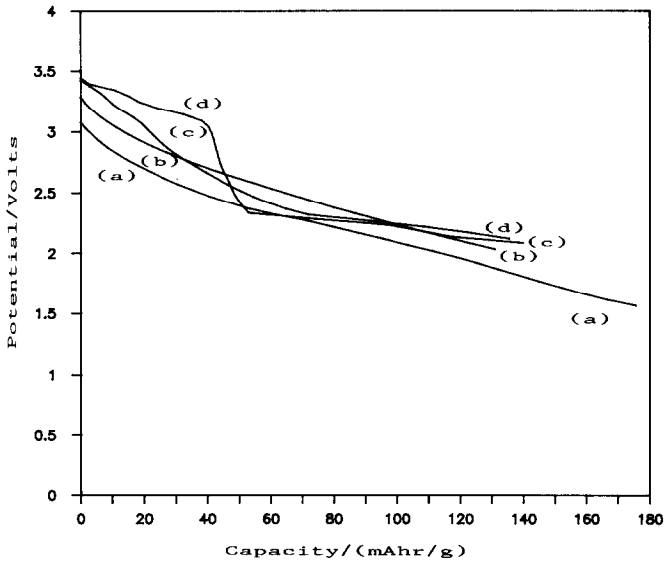

Fig. 9. Variation of cell capacities with annealing temperature (a) 120, (b) 250, (c) 400, (d), 600 °C for mixed titanium/vanadium oxide (53 mol% Ti) cells discharged at 0.033 mA cm^{-2}.

TABLE 6

Summary of cell cycling data for mixed vanadium/titanium oxide (53 mol% Ti) prepared at different annealing temperatures (0.333 mA cm^{-2} discharge, 0.083 mA cm^{-2} charge; 3.2 - 1.7 V)

Annealing temperature (°C)	*OCV* (initial) (V)	Capacity (mA h g^{-1})		
		Cycle 1	Cycle 10	Cycle 24
120	3.487	128	95	92
400	3.585	133	145	132
600	3.493	130	122	120

increased, there was a transition in the shape of the discharge curve, from the step shape for 100% crystalline V_2O_5, to smoother curves associated with amorphous compounds. This appears to be associated with a trend of decreasing capacity. Constant current cycling experiments (Table 7) gave the same capacity trends. The increasing capacity with vanadium content is presumably due to the higher capacity which could be achieved with single vanadium oxide cells in comparison to titanium oxide. However, it is interesting to note that the sharp decreases in capacity on cycling were not observed in any of the cells containing titanium oxide.

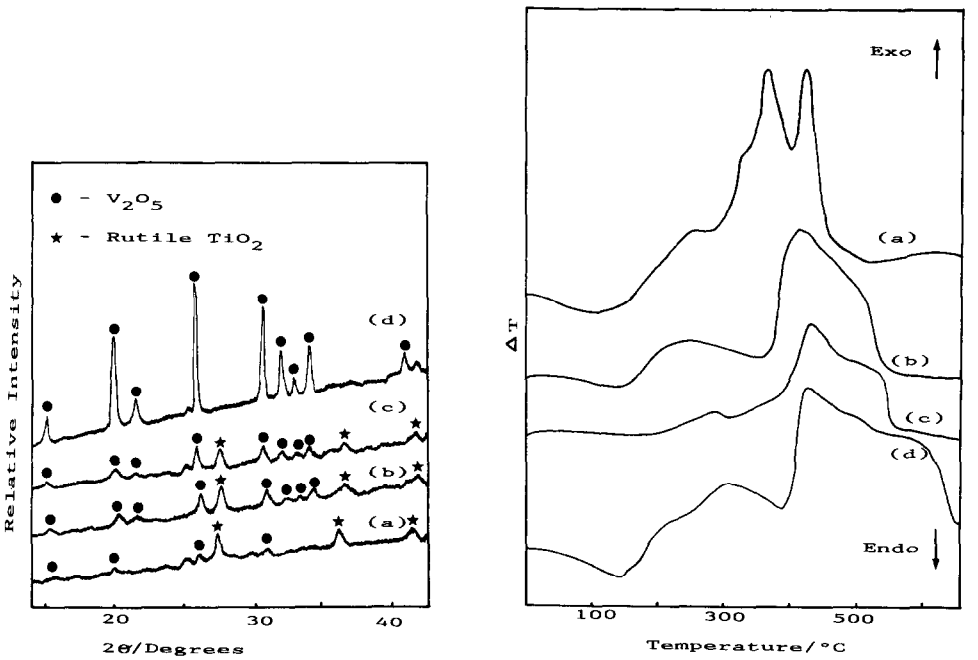

Fig. 10. Change of X-ray diffraction pattern with mol% titanium for mixed vanadium/titanium oxides annealed at 400 °C; (a) 53, (b) 27, (c) 11, (d) 0 mol% Ti.

Fig. 11. DTA curves of mixed vanadium/titanium oxides: (a) 0, (b) 11, (c) 27, (d) 53 mol% Ti.

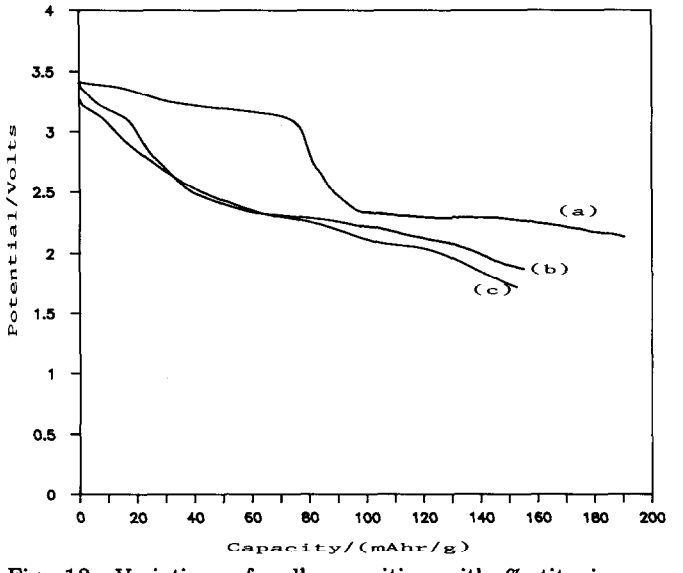

Fig. 12. Variation of cell capacities with % titanium content for mixed titanium/vanadium oxide cells annealed at 400 °C; (a) 0%, (b) 11%, (c) 53% Ti.

TABLE 7

Summary of cell cycling data for mixed vanadium/titanium oxides with different titanium content (0.333 mA cm^{-2} discharge, 0.083 mA cm^{-2} charge; 3.2 - 1.7 V)

Titanium content (mol%)	*OCV* (initial) (V)	Capacity (mA h g^{-1})		
		Cycle 1	Cycle 10	Cycle 25
0	3.494	475	232	224
11	3.612	171	183	180
27	3.580	160	170	168
53	3.533	100	129	126

3.3.4. Comparison of results for sol–gel oxides with V_6O_{13}

Table 8 illustrates the comparison of cycling results from some selected oxides with V_6O_{13}. The results obtained for V_6O_{13} are in agreement with those reported by other workers for comparable cycling regimes in a similar cell design [5, 6, 8]. The capacities obtained from the sol–gel oxides are competitive with, and in some cases superior to, those obtained from V_6O_{13}. In particular, a lower decline in capacity with cycle number can be noted for the cells containing sol–gel oxides (with the exception of the very large capacity drop which occurred on the first cycle in the case of the V_2O_5 cells). The highest first and subsequent cycling capacities were obtained from V_2O_5; this result apparently contradicts the generally held view that V_6O_{13} has the highest cycling capability of all the vanadium oxides. As in all cell cycling experiments the capacities quoted do not represent the theoretically achievable capacity, but only the kinetically achievable capacities under a particular discharge regime. The apparently anomalous result here is due to the use of relatively high current densities. This point may be effectively illustrated with reference to Table 9 which shows the variation of cell capacities for successive cycles with a range of current densities (the results were measured on cells which had already been cycled 20+ times and had reached fairly steady cycling capacities; the charge current was maintained at

TABLE 8

Comparison of cycling capacity of sol–gel oxides with V_6O_{13}

Material	Cycling limits (V)	Capacities (mA h g^{-1}) (0.333 mA cm^{-2} discharge)	
		Cycle 1	Cycle 25
V_6O_{13}	3.2 - 1.7	225	147
Anatase TiO_2	3.0 - 1.7	60	90
Crystalline V_2O_5	3.2 - 1.7	475	224
Amorphous V/Ti (11 mol% Ti)	3.2 - 1.7	171	180
Amorphous V/Ti (53 mol% Ti)	3.2 - 1.7	100	126

TABLE 9

Variation of cell cycling capacities with discharge current density; results shown are for four successive cycles on cells which had reached a steady cycling capacity after approximately 20 cycles (0.083 mA cm^{-2} charge current, 3.2 - 1.7 V).

Material	Capacity (mA h g^{-1})			
	0.333 mA cm^{-2}	0.667 mA cm^{-2}	0.167 mA cm^{-2}	0.333 mA cm^{-2}
100% V	224(0.96)	179(0.76)	234	222
89% V/11% Ti	188(0.95)	137(0.69)	199	187
73% V/27% Ti	142(0.95)	117(0.78)	149	141
47% V/53% Ti	129(0.96)	98(0.73)	134	130
V_6O_{13}	139(0.84)	74(0.45)	165	136

the same value in all cases). As expected, a reduction in capacity with increase in discharge current can be seen in all cases. If the capacities at 0.333 and 0.667 mA cm^{-2} are expressed as a function of the capacity achieved at 0.167 mA cm^{-2} (numbers in brackets in Table 9) it can be seen that, as a percentage, the falls in capacity of the mixed vanadium/titanium oxides are all quite similar, but that the V_6O_{13} cell capacity diminishes more rapidly. These results demonstrate that oxides prepared by the sol–gel technique have a superior rate capability in comparison to this particular V_6O_{13} sample.

4. Conclusions

The sol–gel technique has been demonstrated as a suitable method for the preparation of single and mixed oxides of titanium and vanadium for use as lithium insertion electrodes in polymeric electrolyte cells. The capacity of the titanium oxides was lower than that of the vanadium oxides. On addition of titanium to vanadium in mixed oxide systems, crystallisation processes were suppressed with the resulting oxides exhibiting only minimal capacity losses on cycling in comparison to vanadium oxide alone. In comparative tests with V_6O_{13}, improved rate capabilities were noted for the oxides prepared by sol–gel. It was not clear from the results whether this improved rate performance was an inherent property of the oxides or merely the effect of a smaller particle size and improved dispersion of the oxide in the acetylene black/PEO binder. However, the capacity achieved clearly demonstrates the potential advantages of the sol–gel technique as a route to the production of high rate insertion materials.

Acknowledgements

Financial support for this work by Chloride Advanced Research (Swinton, Manchester) and the Science and Engineering Research Council is

gratefully acknowledged. The authors wish to thank Barry Culpin of Chloride for useful discussions.

References

1 K. M. Abraham and S. B. Brummer, in J. P. Gabano (ed.), *Lithium Batteries*, Academic Press, New York, 1983, p. 371.
2 D. W. Murphy, *Solid State Ionics, 18/19* (1986) 847.
3 M. Armand, J. M. Chabagno and M. Duclot, in P. Vashista, J. N. Mundy and G. K. Shenoy (eds.), *Fast Ion Transport in Solids*, North-Holland, Amsterdam, 1978, p. 131.
4 B. C. H. Steele, G. E. Lagos, P. C. Spurdens, C. Forsyth and A. D. Foord, *Solid State Ionics, 9/10* (1983) 391.
5 A. Hooper, J. S. Lundsgaard and J. R. Owen, *Proc. 3rd Contractors Meet., Talence, France, EUR/8660 EN 53*, Commission European Communities, B.P. 1003, Luxembourg.
6 M. Gauthier, D. Fauteux, G. Vassort, A. Belanger, M. Duval, P. Ricoux, J.-M. Chabagno, D. Muller, P. Rigaud, M. B. Armand and D. Deroo, *J. Electrochem. Soc., 132* (1985) 1333.
7 F. Bonino, M. Ottaviani, B. Scrosati and G. Pistoia, *J. Electrochem. Soc., 135* (1988) 12.
8 M. Z. A. Munshi and B. B. Owens, *Solid State Ionics, 26* (1988) 41.
9 K. West, B. Zachau-Christiansen, M. J. L. Ostergard and T. Jacobsen, *J. Power Sources, 20* (1987) 165.
10 B. C. H. Steele, in C. A. C. Sequeira and A. Hooper (eds.), *Solid State Batteries, Proc. NATO Adv. Study Inst. Solid State Batteries, Alcabideche, Portugal, Sept. 1984*, Nato ASI Series E101, Martinus Nijhoff, Dordrecht, 1985, p. 93.
11 J. J. Auborn, Y. L. Barberio, K. J. Hanson, D. M. Schliech and M. J. Martin, *J. Electrochem. Soc., 134* (1987) 580.
12 O. Yamamoto, Y. Takeda, R. Kanno, Y. Oyabe and Y. Shinya, *J. Power Sources, 20* (1987) 151.
13 Y. Sakurai and J. Yamaki, *J. Electrochem. Soc., 135* (1988) 791.
14 A. C. Leech, J. R. Owen and B. C. H. Steele, *Solid State Ionics, 9/10* (1983) 645.
15 T. Hirai, S. Okada and J. Yamaki, *Proc. Electrochem. Soc. Jpn., H121* (1986).
16 M. Uchiyma, S. Slane, E. Plichta and M. Salomon, in J. P. Gabano, Z. Takehara and P. Bro (eds.), *Proc. Symp. Primary and Secondary Lithium Batteries; Electrochem. Soc., 88-6* (1988) 540.
17 D. R. Ulrich, *J. Non-Cryst. Solids, 100* (1988) 174.
18 J. P. Boilot, P. H. Colomban and N. Blanchard, *Solid State Ionics, 9/10* (1983) 639.
19 M. G. Minett and J. R. Owen, *J. Power Sources, 28* (1989) 397.
20 H. Hirashima, S. Kamimura, R. Muratake and T. Yoshida, *J. Non-Cryst. Solids, 100* (1988) 394.
21 G. Busca, P. Tittarelli, E. Tronconi and P. Forzatti, *J. Solid State Chem., 67* (1987) 91.
22 C. J. Pryor, B. Culpin and M. W. Pilling, in T. Keily and B. W. Barter (eds.), *Power Sources 12*, International Power Sources Symposium, Leatherhead, U.K., 1989, p. 507.
23 L. J. Van der Pauw, *Philips Res. Rep., 13* (1958).
24 *J.C.P.D.S., Powder Diffraction File*, 21-1272.
25 *J.C.P.D.S., Powder Diffraction File*, 21-1276.
26 D. W. Murphy, R. J. Cava, S. M. Zahurak and A. Santoro, *Solid State Ionics, 9/10* (1983) 413.
27 T. Ohzuku, T. Kodama and T. Hirai, *J. Power Sources, 14* (1985) 153.

28 Z. Takehara, T. Nishimura and I. Makino, *New Mater. New Processes, 3* (1985) 259.
29 K. Kanamura, K. Yuasa and Z. Takehara, *J. Power Sources, 20* (1987) 127.
30 *J.C.P.D.S., Powder Diffraction File,* 9-387.
31 J. Bullot, O. Gallais, M. Gauthier and J. Livage, *Appl. Phys. Lett., 36* (1980) 986.
32 N. Kumagai, K. Tanno, T. Nakajima and N. Watanabe, *Electrochim. Acta, 28* (1983) 17.
33 K. Wiesener, W. Schneider, D. Ilic, E. Steger, K. H. Halmeier and E. Brackmann, *J. Power Sources, 20* (1987) 157.